PHYSICAL REVIEW B VOLUME 2, NUMBER 10 15 NOVEMBER 1970

Comparison of Lattice-Parameter and Resistivity Change in Electron-Irradiated Aluminum

H. Wagner, F. Dworschak, and W. Schilling
Institut für Festkörperforschung der Kernforschungsanlage Jülich, Jülich, Germany
(Received 19 June 1970)

Lattice-parameter and residual-resistivity measurements were performed on high-purity aluminum samples irradiated simultaneously with 3-MeV electrons at 4.5 °K. For the lattice-parameter measurements, a rotating single-crystal backreflection x-ray technique with monochromatic radiation (Cu $K\alpha_1$) was used with a resolution of $\Delta a/a \approx 6.5\times10^{-6}$. In four runs the ratio $\eta = (\Delta a/a)/\Delta\rho$ was determined as a function of defect concentration and of thermal recovery. During defect production the ratio η amounts to $(1.61\pm0.10)\times10^{3}$ $(\Omega\,\mathrm{cm})^{-1}$ and remains unaffected by the radiation annealing processes up to defect densities of about 2×10^{-3}. Furthermore, the ratio η stays constant throughout the recovery stages I, II, and III. This behavior suggests that the rearrangement in the local distribution of the interstitials and vacancies accompanying the radiation annealing and thermal recovery processes – especially the interstitial clustering processes – does not appreciably affect the lattice-parameter expansion and the electrical resistivity per unit of Frenkel-defect concentration.

I. INTRODUCTION

Point defects introduced in metals by irradiation with fast particles are usually investigated by residual-electrical-resistivity measurements. Unfortunately, the resistivity increment per unit concentration of Frenkel defects[1] is not known, and may further depend on the mutual arrangement of the interstitials and vacancies in the sample.

In order to investigate this influence, a measurement of the absolute number of interstitials or vacancies in the sample would be necessary. Since this is impossible, at present, one tries to get at least indirect information from simultaneous measurements of the electrical resistivity and another physical property of the irradiated sample. For such a procedure the measurements of both lattice-parameter change and resistivity change have the following advantage: The contribution of the interstitial to the lattice-parameter change per Frenkel defect is usually much larger than that of the vacancy. Therefore, we expect the lattice-parameter change per defect to be sensitive primarily to changes in the arrangement of the interstitials, e.g., clustering into di-interstitials or larger interstitial agglomerates. On the other hand, there is good experimental evidence[2] that in many metals both the interstitials and the vacancies contribute about equally to the resistivity per unit concentration of Frenkel pairs. Therefore, we expect that the electrical resistivity per unit concentration of Frenkel defects is sensitive to the clustering of both interstitials and vacancies.

The present investigation was designed to measure *simultaneously* the lattice-parameter change $\Delta a/a$ and the electrical-resistivity change $\Delta\rho$ in aluminum samples irradiated with 3-MeV electrons at 4.5 °K. From these measurements, the ratio $\eta = (\Delta a/a)/\Delta\rho$ has been obtained as a function of the primary-defect concentration up to values where radiation annealing processes become clearly observable.[3] In subsequent annealing experiments, the influence on the ratio η of the different defect configurations present after the various annealing stages has been determined.

II. X-RAY TECHNIQUE

Precise measurements of small lattice expansions have been made by Simmons and Balluffi[4] using a rotating single-crystal backreflection x-ray technique. We have employed such a method with alterations described below. The whole apparatus was designed so that the sample could be irradiated with electrons and x rays at 4.5 °K without changing the alignment of the crystal.

Figure 1 gives a schematic view of the x-ray path. The x rays emerging from a microfocus tube (line source) (XS), are refocused by a bent quartz monochromator (MO) in the focal line (FO) on the Rowland circle (RC_1). The monochromator was aligned such that only Cu $K\alpha_1$ radiation was reflected. The divergent beam emerging from the focal line (FO) illuminated the whole sample (SP) (12×20 mm^2). However, only that part of the sample where the Bragg condition was fulfilled (a vertical stripe of about 2-mm width) gave rise to a reflected beam with the angle α which was recorded by the film (FL). In the case of Cu $K\alpha_1$ radiation and a (333) reflection in aluminum at 4.2 °K, the angle $\alpha = 180^\circ - 2\theta$ was about 14°, with θ equal to the Bragg angle. During the film exposure the crystal was oscillated approximately 2° with constant angular velocity about a vertical axis passing through the sample. Thus, all parts of the sample were successively placed into Bragg positions which assured

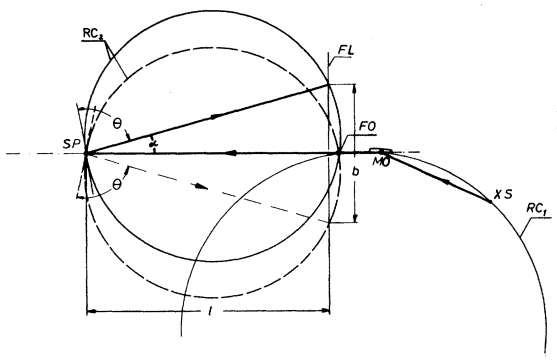

FIG. 1. Schematic diagram of the x-ray path. XS, x-ray source; MO, monochromator; FO, focal line; RC_1, Rowland circle of the monochromator; SP, specimen; FL, film; RC_2, Rowland circle of the oscillated specimen; θ, Bragg angle; α, angle between incident and diffracted beam; b, distance between the two recorded Bragg reflexes; l, specimen-to-film distance. Dashed lines give the arrangement after rotating the specimen through the angle α.

that the entire sample contributed to the observed exposure line and that possible variations in the crystal orientation caused by bending or mosaic structure did not lead to systematic errors. In order to get focusing of the reflected beam on the film, the positions of the sample (SP), the film (FL), and the focal line (FO) were arranged so that they defined a Rowland circle (RC_2), the center of which lay on the bisection of the angle α between incident and diffracted beam.

After one exposure the sample was rotated by the angle α into a position symmetrical to the path of the incoming x rays, as indicated in Fig. 1. In this new position the sample was again oscillated, and a second exposure was made on the film. Therefore, on one film two traces of the diffracted x-ray beam comparable to parts of the Debye-Scherrer pattern were obtained. The change in the distance b between the two recorded lines is related to the relative lattice-parameter change $\Delta a/a$ as follows:

$$\frac{\Delta a}{a} = \frac{1}{4l} \frac{\cos^2(2\theta)}{\tan\theta} \Delta b, \quad \text{with} \quad \tan(2\theta) = -\frac{b}{2l} \qquad (1)$$

and l the distance between specimen and film.

For our experimental arrangement and for the Bragg angle cited above, the resolution $\Delta b/(\Delta a/a)$ was about 1.5×10^3 cm.

By exposure to an illuminated square lattice having a division of 0.1 mm, identical reference marks have been introduced on all films before each x-ray exposure. This procedure eliminated any influence of film-shrinkage effects which may occur during processing of the films.

The width of the recorded lines is mainly due to the natural spectral width of the Cu $K\alpha_1$ emission line and amounts to about 2 mm in the present experimental arrangement. The height of the exposure lines (3 cm) is determined by the linear dimension of the focus of the x-ray tube and by the vertical angular divergence of the monochromator.

The procedure for the determination of the positions of the exposure lines on the films was as follows: First, the films were projected on a wall yielding a magnification of about 15×. Then, the positions of the maximum density of the exposure lines relative to the reference lattice were visually determined at five different heights of the line. The average of these readings was used to define the position of the exposure line on the film.

III. CRYOSTAT

The irradiations were performed at the low-temperature electron-irradiation facility at Jülich, described in detail elsewhere.[5] Excellent cooling conditions are obtained by immersing the samples directly into a stream of liquid helium. This technique allows the irradiation of large specimen areas at 4.5 °K with high electron-beam densities, so that large defect concentrations can be obtained in a reasonable amount of time. The main part of the cryostat is the sample chamber (SC) shown in Fig. 2. The sample (SP) is placed in a flow channel for the liquid helium between two windows (WN) (50-μ $AlMg_3$ foils) which absorb only a small part of the electron and the x-ray beam. The sample chamber was connected to the top of the cryostat by a stainless-steel tube. Through this tube, by means of a suitably constructed sample holder, the speci-

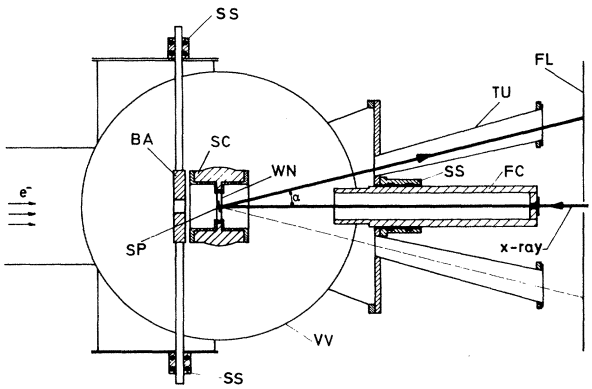

FIG. 2. Horizontal section through the cryostat. SP, specimen; SC, sample chamber defining the flow channel for the liquid helium; WN, sample-chamber windows; BA, electron-beam aperture; VV, vacuum vessel; SS, vacuum-tight slip seal; FC, Faraday cage; TU, exit tubes for the diffracted x rays; FL, film; α, angle between incident and diffracted beam. Dashed line shows the diffracted x-ray beam after the rotation of the specimen through the angle α.

mens could easily be inserted into the flow channel. A 10-cm-long piece of Invar tube connected the sample chamber rigidly to a cross-slide at the bottom of the cryostat. This cross-slide was used for the final alignment of the sample in the chamber after cooling down to 4.5 °K. A detailed description of the whole cryostat is given in Ref. 6.

A water-cooled beam aperture (BA) (Fig. 2) defined an area which was large enough so that the single-crystal specimen (SP) was irradiated over its full width (12 mm) and a length of 20 mm. The electron beam was stopped in a Faraday cage (FC) which could be moved directly behind the sample chamber during the electron irradiation. The bottom of the cage was vacuum sealed by a 50-μ $AlMg_3$ window and covered with a water-cooled copper plate from the outside. This plate served as a beam stop during the electron irradiation and could be removed during the x-ray measurements, so that the x rays could enter the cryostat through the window in the Faraday cage. In addition, during the x-ray exposure the cage could be withdrawn from the sample chamber so that it did not obstruct the path of the diffracted x-ray beam. This position is shown in Fig. 2. The diffracted beam could leave the cryostat through the tubes (TU), the ends of which were vacuum sealed with 100-μ-thick Mylar foils.

For annealing the samples, the flow of liquid helium by-passed the sample chamber which was heated by an electrical heater.

IV. SAMPLE PREPARATION AND MOUNTING

A rectangular single-crystal bar having a ⟨111⟩ axis as the rod axis was grown from 99.999+% pure aluminum obtained from AIAG Metals Inc., New York. This bar was spark cut into 1-mm-thick slices with surfaces parallel to a (111) plane. The sides of these rectangular slices were cut away and used to prepare specimens for electrical-resistivity measurements. After annealing at 400 °C for 2 h in a vacuum ($<10^{-5}$ Torr), the resistivity ratio $R=\rho_{273\,^\circ K}/\rho_{4.2\,^\circ K}$ of the mounted specimens was found to be about 3000.

The slices of aluminum ($12\times25\ mm^2$) were thinned to a final thickness of about 0.1 mm and were mounted on aluminum frames. The upper end of the samples was rigidly clamped into the frame, whereas the lower end was allowed to move freely during thermal contraction and radiation-induced elongation of the foils. The frame, together with the specimen, could be oscillated with respect to the sample holder with a maximum angle of rotation of about ±9°.

V. ERROR ANALYSIS

Errors in the determination of the distances b and l and a systematic vertical tilting of the crystal can lead to errors in the measured lattice-parameter change $\Delta a/a$, according to Eq. (1). Ideally, the atomic planes diffracting the x rays must be parallel to the axis of rotation of the crystal. When these planes are tilted out of the axis of rotation by an angle γ, the distance b between the two recorded lines decreases. Hence, an apparently increased Bragg angle θ' is measured, which is related[7] to the true Bragg angle θ by

$$\sin\theta=\sin\theta'\cos\gamma\ . \tag{2}$$

We could reduce the tilt angle γ to less than 1° by a final alignment of the sample in the cryostat. Considering possible errors in b, l, and γ, we obtain with Eqs. (1) and (2) the difference between the true and the observed lattice-parameter change:

$$\delta\frac{\Delta a}{a}=\left(\frac{\Delta a}{a}\right)_{true}-\left(\frac{\Delta a}{a}\right)_{observed}$$

$$=\tan\gamma\delta\gamma+\frac{b}{2l^2}\ \frac{\delta b+(b/l)\delta l}{\left[\frac{1}{2}+(b^2/l^2+4)^{-1/2}\right](b^2/l^2+4)^{3/2}}\ . \tag{3}$$

For $\gamma=1°$, $l=400$ mm, and $b=200$ mm, Eq. (3) becomes

$$\delta\Delta a/a=1.7\times10^{-2}\delta\gamma+7.2\times10^{-5}(\delta b+0.5\delta l)\ . \tag{3'}$$

Possible systematic errors resulting from an eccentric placement of either the specimen or the incident x-ray beam relative to the axis of rotation, from finite specimen height, and from absorption in the specimen, can be neglected.

The following types of errors limit the accuracy of the determination of $\Delta a/a$:

(i) *Random errors.* Since the distance between the two recorded lines could be determined with an accuracy $\delta b=0.07$ mm, and further errors can arise due to changes of the specimen-film distance l (we have estimated this distance to be constant within 0.015 mm during one experimental run), we calculate the contribution of all random errors to be about 6.5×10^{-6}.

(ii) *Constant systematic errors.* Errors which are constant during one experimental run arise from limitations in the accuracy of the determination of the absolute values b and l, the only quantities which enter into the determination of the Bragg angle θ. The absolute value b was determined with an accuracy of 0.5%, whereas the distance l could only be measured with an accuracy of 1% because the specimen was not accessible in the sample chamber. A better determination of the distance l by means of the well-known lattice parameter of aluminum at 4.5 °K and the Bragg law is not possible because the tilt angle γ is not known to be better than 1°. These errors limit the accuracy in the determination of the absolute value of $\Delta a/a$ to about 2.5%.

(iii) *Variable systematic errors.* Systematic changes of the specimen-film distance l and the tilt angle γ during one experimental run can cause fictitious lattice-parameter changes. Such systematic errors can occur if the lower end of the specimen cannot move freely in its frame. Then the irradiation-induced elongation can lead to a S-shaped flexure of the single-crystal foils. This effect gives rise to a continuous change of the angle γ, thereby pretending an additional lattice-parameter change [see Eq. (3)]. From the continuous lengthwise shifting of the Bragg lines during runs II and III of the experiments reported later, we must conclude that such an effect indeed occurred during these runs. From this shift, the maximum change $\delta\gamma$ of the tilt angle can be estimated to be about $\frac{1}{4}°$. For $\gamma \approx 1°$ this would correspond to systematic errors of about 10% in the determination of $\Delta a/a$.

VI. EXPERIMENTAL RESULTS

A total of four irradiation runs were made using four different sets of samples. In each run one sample for the lattice-parameter measurement and one sample for the electrical-resistivity measurement were irradiated simultaneously. The electron energy was 3.0 MeV, the beam density was 40 $\mu A/cm^2$ and was homogeneous to ± 3% across both specimen areas. Typical dose curves observed for the electrical resistivity as well as for the lattice-parameter change are shown in Fig. 3. As

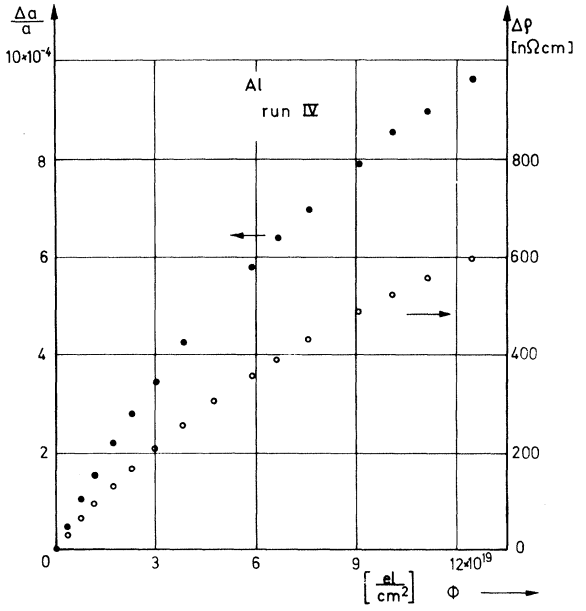

FIG. 3. Dose curve of run IV. Open circles are the data of resistivity measurements; full circles are the data of lattice-parameter measurements. Deviation from the straight line in both curves is caused by saturation effects.

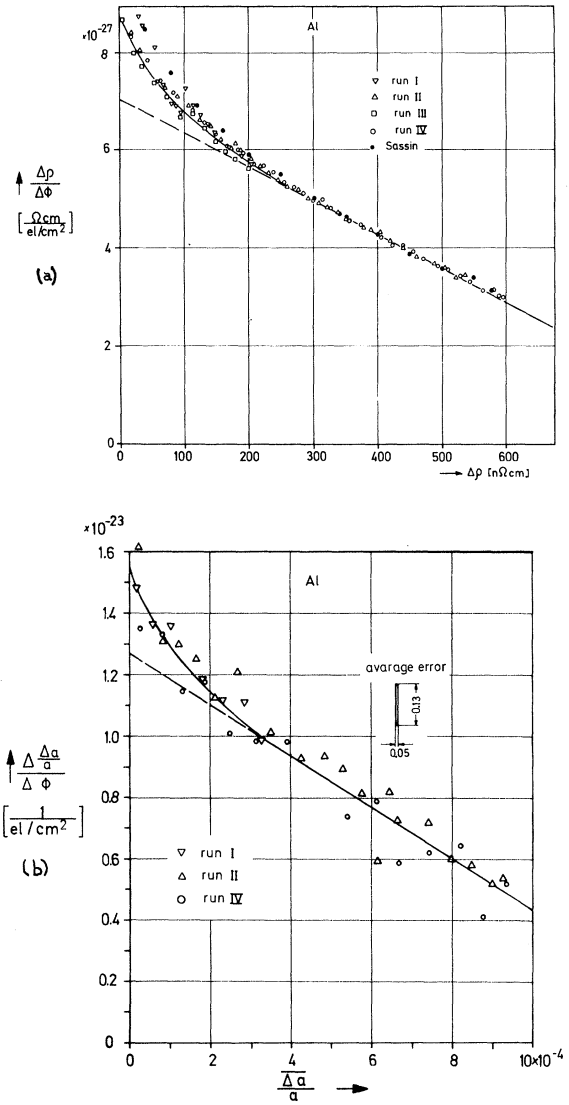

FIG. 4. (a) Resistivity damage rate versus total resistivity increase during electron irradiation of aluminum at 4.5 °K. Only half of the measured data have been plotted and a few data from Ref. 3. (b) Rate of lattice-parameter change versus total increase of the lattice parameter during electron irradiation of aluminum at 4.5 °K. Plotted data have been obtained by point-by-point differentiation of the observed dose curves.

can be seen from these curves, the damage rates determined by both types of measurements decrease continuously with increasing irradiation dose.

This saturation behavior is outlined more clearly in Figs. 4(a) and 4(b), where the incremental-resistivity and lattice-parameter increase per unit dose are plotted versus the irradiation-induced defect density as determined from the total irradiation-induced resistivity and lattice-parameter change, respectively.

By extrapolating this decrease to the damage-rate zero, we obtain the saturation value

$$\Delta\rho_\infty = 995 \pm 10 \text{ n}\Omega \text{ cm} .$$

Two mechanisms are responsible for the observed radiation annealing: (a) spontaneous recombination of new interstitials with vacancies produced earlier or vice versa, and (b) recombination of close Frenkel pairs by nearby subthreshold recoil events. A detailed discussion of the radiation annealing in electron-irradiated aluminum has been given in separate publications.[3,8] As shown in Fig. 4(b), the initial nonlinear decrease of the damage rate in electron-irradiated aluminum is also observed by the lattice-parameter measurements, which in turn supports the interpretation given earlier,[8] that the initial nonlinear decrease of the damage rate is not due to a decrease of the electrical resistivity with increasing Frenkel-defect concentration.

In Fig. 5 the total irradiation-induced lattice-parameter change has been plotted versus the irradiation-induced electrical-resistivity change. If the ratio $\eta = (\Delta a/a)(\Delta\rho)^{-1}$ is independent of the defect density introduced by the irradiation, one straight line is expected for all runs in this plot. Experiments I and IV do, in fact, yield straight lines with identical slopes. However, the data for the other two runs show slight deviation from linearity and different slopes. Since the statistical error of each data point amounts to the size of the symbols used in Fig. 5, a systematic error which increases with irradiation dose and varies between the different irradiations must cause these deviations. We have found a continuous vertical shift of the Bragg lines recorded on the film during runs II and III which was not observed during runs I and IV. This shift indicates a continuous vertical tilting of the crystal giving rise to a systematic error as discussed in Sec. V.

Since the initial value of the misorientation γ was not known precisely for the different samples, we were unable to correct for this effect quantitatively using Eq. (3). Therefore, for a further evaluation of the ratio η we did not use the results of runs II and III.

The analysis of the data of the experiments I and IV shows that the ratio η is constant within experimental error up to the largest irradiation-induced defect densities investigated (600 nΩ cm) and amounts to

$$\eta = (1.61 \pm 0.10) \times 10^3 \ (\Omega \text{cm})^{-1} .$$

The error given above is composed of the statistical error which was found to be 3% plus the constant systematic error of 2.5%. The ratio η has been determined by other authors and their results are compiled in Table I for comparison.

When comparing these results we have to consider that Isebeck *et al.*,[2] Himmler *et al.*,[10] and Hanada *et al.*[11] did not measure the resistivity increase simultaneously with either length or lattice-parameter change. Therefore, the known difficulties in the dose measurements and calibration enter directly into the evaluation of their values of η. Only the ratio η in Blewitt's experiment[9] was determined by simultaneous measurements of both properties, but the sample was not pure aluminum. In addition, only one irradiation run has been performed in each of the experiments mentioned above. Therefore, possible systematic errors could not be detected.

After each irradiation run, the samples were annealed isochronally for 15 min at temperature intervals ΔT given by $\Delta T/T = 0.15$ and 0.5 for the high- and low-dose experiments, respectively. After each annealing step the samples were again cooled to 4.5 °K, where resistivity and lattice-parameter measurements were performed. The results are shown in Fig. 6(a) for the low-dose runs I and III and in Fig. 6(b) for the high-dose runs II and IV.

As can be seen from the normalized recovery curves, the electrical-resistivity and lattice-parameter changes coincide within experimental error. We conclude that the ratio η is equal for all recovery stages I, II, and III in aluminum. This statement holds for both the low- and the high-dose experiments[12] and confirms the earlier results after neutron[10] and fission-fragment[9] irradiation.

A comparison of the data of Figs. 6(a) and 6(b) shows that at defect densities which approach the saturation concentration, the total recovery in stages II and III increases strongly at the expense of the recovery in stage I. In general, the overall appearance of the recovery curves at very high electron doses closely resembles the recovery of

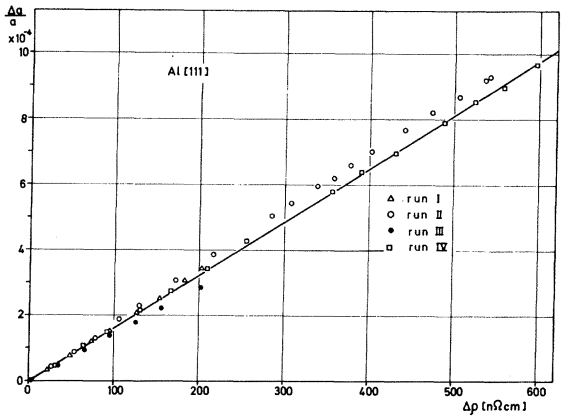

FIG. 5. Lattice parameter versus resistivity increase caused by electron irradiation at 4.5 °K. The straight line is calculated from run IV. Its slope gives the ratio $(\Delta a/a)/\Delta\rho = (1.61 \pm 0.10) \times 10^3 \ (\Omega\text{cm})^{-1}$.

TABLE I. Collected experimental values of the ratio η of the lattice-parameter change $\Delta a/a$ to the resistivity change $\Delta\rho$.

Particles	η $10^3 \times (\Omega\,\mathrm{cm})^{-1}$	Number of runs	Method[a]	Authors
Fission fragments[b]	1.23	1	L	Blewitt (Ref. 9)
Neutrons	1.20 ± 0.05	1	L	Isebeck *et al.* (Ref. 2)
Neutrons	1.3 ± 0.2	1	A	Himmler *et al.* (Ref. 10)
Electrons	0.9 ± 0.3	2	L[c]	Hanada *et al.* (Ref. 11)
Electrons	1.61 ± 0.10	4[d]	A	This work

[a] L, length measurements; A, lattice parameter measurements.

[b] Al + 0.1% U^{235}.

[c] Comment by the authors: "The damage rate results of aluminum were poor."

[d] The ratio η was determined from these two runs which were not affected with variable systematic errors.

neutron-irradiated aluminum. These observations are in complete agreement with earlier measurements.[13] Further details of the recovery of aluminum and the mechanisms which are responsible for the change of the annealing structure with increasing dose have been discussed elsewhere.[14]

VII. DISCUSSION

If a cubic crystal of finite size contains point defects, the positions and orientations of which are distributed at random, and if the displacement fields around the individual defects superpose additively, the relative change $\Delta a/a$ of the average interatomic distance in the crystal is given by[15]

$$\Delta a/a = \tfrac{1}{3} c P/K \,, \tag{4}$$

where c is the volume concentration of the defects, K the bulk modulus, and P is a quantity which can be derived from the interaction potential of the defect atom with its neighboring atoms.[16]

Detailed model calculations performed for Cu by two different investigators gave values for the relative volume change per interstitial of 1.4 [17,18] and 2.2 atomic volumes,[19,20] respectively. Both values have been found to be equal within 20% for the different (eventually metastable) interstitial configurations investigated and to be rather insensitive to the choice of the interatomic potential.[21] Vacancies's values $\Delta V/V$ between -0.1 and -0.3 have been calculated.[17,19,20] Although similar calculations are not available for aluminum, one would expect that also for this metal the relative volume change for interstitials is larger by an order of magnitude than it is for vacancies. Therefore, the observed change in the lattice parameter in irradiated samples is due mainly to the presence of interstitials, whereas the vacancies contribute very little.

On the other hand, there is good theoretical and experimental evidence[2] that vacancies and interstitials contribute about equally to the resistivity per unit concentration of Frenkel pairs. If the total resistivity and lattice-parameter change per unit concentration of Frenkel defects is separated into the contribution of vacancies and interstitials, one obtains

$$\eta = \frac{1}{3\Omega_0 K} \frac{P_i + P_V}{\Delta\rho_i + \Delta\rho_V} \,, \tag{5}$$

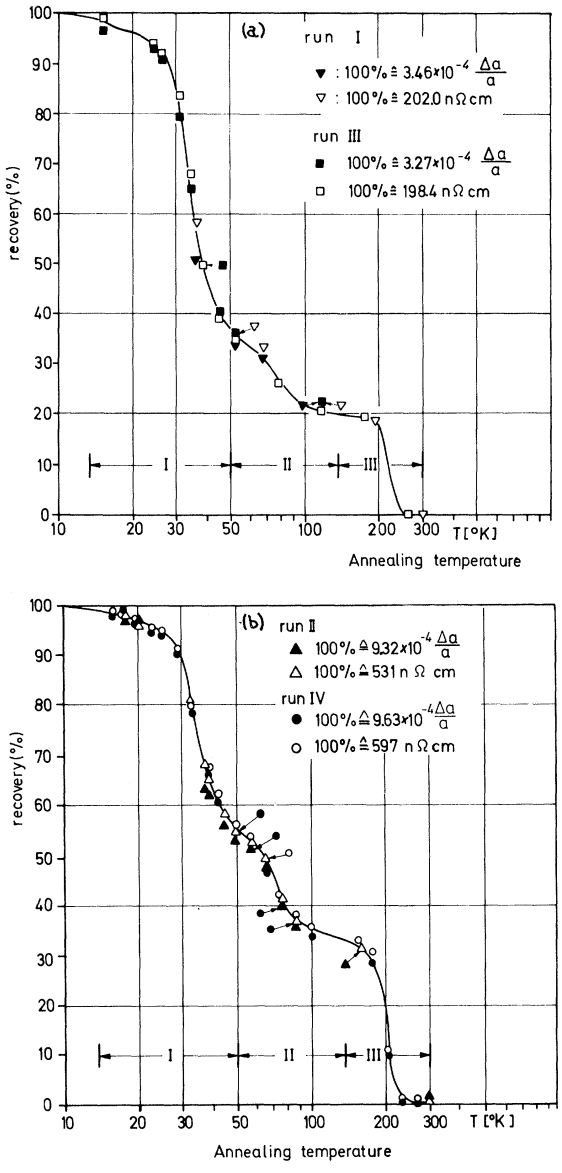

FIG. 6. Isochronal recovery curves of the lattice parameter and the resistivity change: (a) after low-dose electron irradiation at 4.5 °K; (b) after high-dose electron irradiation at 4.5 °K. The recovery is given in % of the values at the end of the irradiation.

where Ω_0 is the atomic volume and the indices i and V characterize the contribution per unit atomic concentration of interstitials and vacancies to P and $\Delta\rho$, respectively. As stated above, $|P_i| \gg |P_V|$ and $\Delta\rho_i \approx \Delta\rho_V$. Therefore, during any clustering process, e.g., of the interstitials, η can remain constant only if both P_i and $\Delta\rho_i$ remain constant or if the relative change in P_i during the clustering process is approximately twice as large as the relative change in $\Delta\rho_i$.

As discussed in Sec. VI, for aluminum the ratio η is constant within experimental error during defect production at 4.5 °K up to defect densities where saturation effects are rather pronounced. Using Eq. (5), the observed constancy of the ratio η can then be interpreted by the assumption that both $P_i + P_V \approx P_i$ and $\Delta\rho_i + \Delta\rho_V$ are not affected appreciably by the radiation annealing processes. In principle, it could also be true that P_i changes just as much as $\Delta\rho_i + \Delta\rho_V$. However, this would be a rather special case and seems to be less probable than the approximate constancy of P_i and $\Delta\rho_i + \Delta\rho_V$. In the final stage these saturation effects are known to be accompanied by a strong tendency for interstitial and vacancy coagulation, so that ultimately the whole crystal should break up into regions with high preferential vacancy or interstitial population.[22,23] However, no estimate of the exact magnitude of the vacancy and interstitial coagulation in our high-dose samples can be given.

During the recovery of the irradiation-induced Frenkel defects, interstitial clustering processes play an important role.[14] Regardless of the special details, all recovery models predict that in pure samples the interstitials can survive above stage I by interaction with each other, thereby forming immobile entities like di-interstitials or pairs of converted interstitials.[14] In any case, above stage I the interstitial distribution will be highly correlated and this correlation is probably further enlarged by the recovery processes within stage II. Again, from the observed constancy of the ratio η throughout recovery stages I–III we can conclude that for aluminum the properties P_i and $\Delta\rho_i$ per interstitial remain further unaffected by the interstitial agglomeration processes occurring in stages I and II.

The conclusion that both the lattice expansion and the electrical resistivity per unit defect concentration of interstitials are rather insensitive to the special arrangement of the interstitials (in form of single defects, di-interstitials, and small clusters) cannot be generalized to other metals. For Cu, for example, rather pronounced differences in the ratio η have been observed within the different recovery stages.[24] No physical argument is known which could explain the good additivity of the defect properties in aluminum.

ACKNOWLEDGMENTS

We wish to thank Dr. H. Hemmerich and his irradiation group and many other members of the institute for their assistance during the irradiation. We are also indebted to Professor R. Hosemann for helpful discussions and to R. H. Kernohan and Dr. W. Sachse for carefully reading the manuscript.

---

[1]Here and in the following, the term "Frenkel defect" is used to denote the existence of an equal number of vacancies and interstitials in the sample, irrespective of their mutual arrangement, whether in the form of single isolated defects, pairs, or clusters.

[2]K. Isebeck, F. Rau, W. Schilling, K. Sonnenberg, P. Tischer, and H. Wenzl, Phys. Status Solidi 17, 259 (1966).

[3]G. Duesing, W. Sassin, W. Schilling, and H. Hemmerich, Crystal Lattice Defects 1, 55 (1969).

[4]R. O. Simmons and R. W. Balluffi, Phys. Rev. 109, 1142 (1958).

[5]H. Hemmerich, W. Sassin, and W. Schilling, Z. Angew. Phys. 29, 1 (1970).

[6]H. Wagner, KFA Jülich Report No. Jül-664-FN, 1970 (unpublished).

[7]W. L. Bond, Acta Cryst. 13, 814 (1960).

[8]G. Duesing, H. Hemmerich, W. Sassin, and W. Schilling, Crystal Lattice Defects 1, 135 (1970).

[9]T. H. Blewitt, in *Radiation Damage in Solids*, edited by D. S. Billington (Academic, New York, 1962).

[10]U. Himmler, H. Peisl, A. Sepp, W. Waidelich, and H. Wenzl, Z. Angew. Phys. 23, 8 (1967).

[11]R. Hanada, C. L. Snead, and J. W. Kaufmann, J. Appl. Phys. 40, 3694 (1969).

[12]Unfortunately, in both irradiations I and III the x-ray samples had been damaged during the isochronal annealing program at about 100 °K by too rapid cooling. Therefore, no data points for the lattice-parameter change are available above this temperature. Nevertheless, the equality of η within stages I and II and, therefore, also within stage III is firmly substantiated by the existing data.

[13]W. Sassin, KFA Jülich Report No. Jül-586-FN, 1969 (unpublished).

[14]W. Schilling, in *Vacancies and Interstitials in Metals*, edited by J. Diehl, W. Schilling, D. Schumacher, and A. Seeger (North-Holland, Amsterdam, 1969).

[15]R. Siems, KFA Jülich Report No. Jül-545-FN, 1968 (unpublished).

[16]K. Fischer and H. Hahn, Z. Physik 172, 172 (1963).

[17]A. Seeger and E. Mann, J. Phys. Chem. Solids 12, 326 (1960).

[18]A. Seeger, E. Mann, and R. v. Jan, J. Phys. Chem. Solids 23, 639 (1962).

[19]R. A. Johnson and E. Brown, Phys. Rev. 127, 446 (1962).

[20]R. A. Johnson, Radiation Effects 2, 1 (1969).

[21]This statement indicates that the difference in the values of $\Delta V/V$ cited above between the calculations of Seeger *et al.* (Refs. 17 and 18) and of Johnson *et al.* (Refs. 19 and 20) are not due to the different potentials

used for the calculations. Instead, it may be because the calculations of Seeger *et al.* (Refs. 17 and 18) allowed for the anisotropy of the dilatation field around the interstitials, whereas the calculations of Johnson assumed an (unrealistic) isotropic displacement field at large distances.

[22]G. Lück and R. Sizmann, Phys. Status Solidi 14, 507 (1966).
[23]J. R. Beeler, Phys. Rev. 150, 470 (1966).
[24]U. Himmler, H. Peisl, A. Sepp, W. Waidelich, and H. Wenzl, Z. Angew. Phys. 28, 175 (1969); Phys. Rev. Letters 19, 956 (1967).

PHYSICAL REVIEW B VOLUME 2, NUMBER 10 15 NOVEMBER 1970

Anisotropic Relaxation Times and Magnetoconductivity for Ellipsoidal Energy Surfaces: Onsager Reciprocity Restrictions and Jones-Zener Expansions

T. D. Fuchser, H. J. Mackey, and J. R. Sybert
Department of Physics, North Texas State University, Denton, Texas 76203
(Received 15 June 1970)

The magnetoconductivity is obtained using anisotropic relaxation-time tensors for materials having Fermi surfaces consisting of a group of ellipsoids. Each ellipsoid is described in terms of a number of carriers and a saturation field tensor. From crystal symmetry and Onsager reciprocity, it is proven in some cases and inferred for all other cases that all saturation field tensors must be symmetric. The anisotropic relaxation-time tensor is thereby restricted, but need not be symmetric itself. The saturation-field-tensor symmetry also requires the existence of ellipsoids of constant power density upon application of an electric field and no magnetic field. The Jones-Zener expansion of the conductivity in terms of magnetic field is simply derived, including anisotropic relaxation-time tensors. The Jones-Zener series diverges to infinity if a critical magnetic field H_c is reached. An expression for H_c is obtained and compared with past criteria for convergence.

INTRODUCTION

Magnetoconductivity theories are common in the literature for semiconductors and semimetals whose constant-energy surfaces are approximated by a group of ellipsoids. Most of these theories have assumed isotropic relaxation times, but lately there has been evidence for anisotropic relaxation times in copper,[1] bismuth,[2] and bismuth telluride.[3] A previous paper by Mackey and Sybert,[4] hereafter called Paper I, used anisotropic relaxation times in the calculation of the conductivity for a group of ellipsoids. Anisotropic relaxation times have also been used in theories for many-valley semiconductors by Herring and Vogt,[5] in theories for bismuth by Hartman[2] and by Samoylovich and Pinchuk,[6] and in theories for bismuth telluride by Korenblit[7] and by Hübner.[3]

The theories for bismuth and bismuth telluride are applicable to the whole group of solids which have ellipsoidal Fermi surfaces, and it is unfortunate that exposure has been restricted to researchers working with these two materials. Thus, it seemed worthwhile to make an extension of Paper I, providing a more comprehensive treatment for the use of anisotropic relaxation-time tensors. At the same time the simplicity of the results is stressed.

Some confusion seems to exist on whether or not to assume the principal-axis system of the relaxation-time tensor coincides with that of the effective-mass tensor. In either case, the principal-axis system of the relaxation-time tensor is restricted by the Onsager reciprocity relation and by crystal symmetry requirements. These restrictions are developed here, and one finds a rather simple physical interpretation of the results.

The theory of Paper I is generalized in this paper by inserting anisotropic scattering into the original Boltzmann transport equation, and by including formulas applicable to semiconductor calculations as well as for the degenerate case. The Jones-Zener series is then derived in matrix form to arbitrary order. From this, the Jones-Zener coefficients which properly include anisotropic relaxation are readily identified. The regions of convergence and divergence of the Jones-Zener series are separated by a "critical" magnetic field strength which is derived and found to be a function of the magnetic field direction.

BOLTZMANN TRANSPORT EQUATION WITH ANISOTROPIC RELAXATION TIME

The Boltzmann transport equation for electrons is

$$\nabla_x f \cdot \vec{v} - \nabla_p f\left(e\vec{E} + \frac{e}{c}\vec{v}\times\vec{H}\right) = \left(\frac{\partial f}{\partial t}\right)_c , \qquad (1)$$

where $e = |e|$ is the electron charge and f is the